

Review

# Review of Material Parameter Calibration Method

Weiquan Fang, Xinzhong Wang \*, Dianlei Han and Xuegeng Chen

School of Agriculture Engineering, Jiangsu University, Zhenjiang 212013, China; 2112116003@ujs.edu.cn (W.F.); handianlei@ujs.edu.cn (D.H.); 1000005204@ujs.edu.cn (X.C.)

\* Correspondence: xzwang@ujs.edu.cn; Tel.: +86-13852989966

**Abstract:** The discrete element method and simulation analysis of the interaction between granular materials and implements provide a convenient and effective method for the optimal design of farming machinery. However, the parameter differences between different materials make discrete element simulation impossible to carry out directly. It is necessary to obtain the specific material parameters and contact parameters through parameter calibration of the simulation object, so as to make the simulation results more reliable. Parameter calibration mainly includes intrinsic parameter measurement, contact model selection, contact parameter selection, and parameter calibration. The test methods of the calibration test include the Plackett–Burman test and other methods of screening parameters with significant influence, and then selecting the optimal parameters through the climbing test, response surface analysis method, etc., and finally carrying out the regression analysis. This paper will describe the existing parameter measurement methods and parameter calibration methods and provide a reference for the scholars who study parameter calibration to carry out parameter calibration.

**Keywords:** discrete element method; contact parameters; parameter calibration



**Citation:** Fang, W.; Wang, X.; Han, D.; Chen, X. Review of Material Parameter Calibration Method. *Agriculture* **2022**, *12*, 706. <https://doi.org/10.3390/agriculture12050706>

Academic Editors: Muhammad Sultan, Redmond R. Shamshiri, Yuguang Zhou and Muhammad Imran

Received: 21 April 2022

Accepted: 16 May 2022

Published: 17 May 2022

**Publisher's Note:** MDPI stays neutral with regard to jurisdictional claims in published maps and institutional affiliations.



**Copyright:** © 2022 by the authors. Licensee MDPI, Basel, Switzerland. This article is an open access article distributed under the terms and conditions of the Creative Commons Attribution (CC BY) license (<https://creativecommons.org/licenses/by/4.0/>).

## 1. Introduction

Since the discrete element method was proposed, it has been widely used to study the contact simulation between tools and granular materials to analyze the contact force between materials and tools, particle force and velocity field analysis, which improves the design efficiency of tools, but discrete element simulation requires accurate parameters to make the simulation results accurate [1]. Accurate parameters need to be obtained through the measurement of intrinsic parameters and literature review. Even if the contact parameters and some intrinsic parameters can be measured by experiments, they still need to be calibrated to ensure their accuracy [2–4].

The parameters of the material include intrinsic parameters and contact parameters. The intrinsic parameters include Poisson's ratio, density, particle shape and radius, shear modulus, and Young's modulus of the particles. The contact parameters include (particle–particle/particle–rigid body) static friction coefficient, (particle–particle/particle–rigid body) rolling friction coefficient, (particle–particle/particle–rigid body) collision coefficient of restitution, and particle–particle contact parameters generally need to be calibrated by establishing the relationship between microscopic parameters and macroscopic tests [5,6]. The simulation result of the interaction between particles will be more realistic when accurate contact parameters are used [7,8]. There are two methods for measuring particle parameters. One is to measure the parameters with a test instrument through experiments directly. The second method is to establish the relationship between microscopic parameters and macroscopic parameters through simulation tests for parameter calibration. Generally, the angle of repose is used for parameter calibration. Auxiliary tests for parameter calibration include the response value, direct shear test, triaxial compression test, and tillage test [9].

Before the parameters are calibrated, it is necessary to select the contact model, and the accumulation angle of the material is often used as the response parameter of the parameter calibration [10,11]. After determining parameters such as particle size and shape during calibration, the Plackett–Burman test, center combination test, and other test methods are used to screen the significant parameters. Furthermore, climbing tests and response surface tests, among others, are required to determine the specific value of the parameters to be calibrated, after which regression analysis between the influence parameters and the response parameters is used to establish the relationship between the calibration parameters and the response parameters [12,13]. The simulation usually adopts the discrete element simulation software EDEM 2020 (creator: DEM Solutions; location source: Edinburgh, England), ROCKY DEM 4.5 (Engineering Simulation S and Scientific Company (ESSS); location source: Sao Paulo, Brazil), PFC 5.0 (creator: ITASCA; location source: Illinois, American) and so on. PFC is mainly used in the field of geotechnical mechanics, with two versions of PFC: 3D and 2D; PFC3D performs well in simulating the tensile of fracturing [14]. ROCKY DEM is used more in fragmentation, and its polyhedron modeling is more accurate, but it takes more time, and it has less reference than EDEM. EDEM is faster in terms of polyhedron calculation, has more reference materials, and has a relatively wide range of applications. Different modeling and simulation methods require the use of different functions. When the required functions are not available in EDEM, API can be written to expand the functions. For EDEM, in post-processing, the function modules can be expanded through EDEMPy to improve the effect and efficiency of post-simulation processing.

This paper will introduce the test methods for parameter calibration, measurement methods of intrinsic parameters, selection of contact models, measurement and calibration of contact parameters, and address existing problems and prospects of parameter calibration.

## 2. Overview of the Test Methods Used for Parameter Calibration

The angle of repose is usually used as a response to material parameter calibration, and the parameters to be calibrated are mainly particle–particle contact parameters. When the specific parameters to be calibrated cannot be determined, the Plackett–Burman test is used to screen the significant factors. The test method and the Box–Behnken test method are used to determine the values of the parameters to be calibrated [15].

Peng C. conducted the Plackett–Burman test based on the software named Design-Expert, eliminated the parameters with insignificant effects, selected the test parameters with more significant effects, used the Design-Expert software to perform multiple regression fitting analysis, and obtained the angle of repose regression equations [16,17]. Based on the central experimental design method, Shi L. established a soil simulation model/contact parameter prediction model, using shear strength and friction coefficient as the parameters to be calibrated, and the Box–Behnken test method for parameter calibration with soil angle of repose as response [18]. Zhang R. used the extremely significant parameters screened by the Plackett–Burman test, used the cylinder lifting simulation test to conduct the steepest climbing test, and the general rotating center combination test was used to calibrate the friction factor of rice grains [19].

Through the Plackett–Burman test, Shi G. found that Poisson's ratio and static friction coefficient are the significant parameters. During calibration of the basic values, the center combination test is performed based on the steepest climbing test to perform parameter calibration to obtain the optimal parameter value. The simulated accumulation angle is compared with the actual test accumulation angle and the error is analyzed. The slope flow simulation and experiment are used to further test the reliability of the results [20,21].

## 3. Measurement Method of Material Intrinsic Parameters

### 3.1. Particle Size and Shape

Particle shape and size are the main factors affecting the angle of repose. It needs to be consistent with the real particles as much as possible. When the particles are small, the

particles are set as spherical particles. If it is larger and regular, the appearance model can be imported into EDEM for API particle filling [22]. If the particle shape is irregular and the particle shape is required, the triaxial size measurement and modeling of the particle are adopted [23,24]. Particles' three-dimensional shape and size can be determined by obtaining point cloud data [25]. It is also possible to use the method of image recognition and edge extraction to obtain the outline of the particles and carry out 3D modeling [26]. The proportions of particles with different radii in the particle system are different, and the proportioning method is adopted for the proportioning of particles with different radii in the simulation [27]. The shape and smoothness of the spherical surface have an influence on the stacking angle. To a certain extent, the more concave and convex the surfaces, the larger the stacking angle [28]. Irregular-shaped particles are filled with spherical particles to form the actual shape. Different filling schemes will lead to inconsistent surface edges and corners and affect the angle of repose.

Particles' size can be determined by the sieving method, laser diffraction, digital image method, densitometer method, pipette method, etc. The sieving method uses sieves with different apertures to vibrate and sieve particles, and it is suitable for particle sieving with a particle size greater than 0.075 mm. The densitometer method, pipette method, laser diffraction, and digital image method are suitable for particle size sieving with a smaller particle size. Laser diffraction and the digital image method are efficient, but their accuracy needs to be verified [29–32]. The particle size and proportion are determined by the sieving method when it is larger and irregular. Particles need to be measured by the three-axis dimensions of the real object to obtain data for modeling, and then use 3D modeling software for modeling and import into software such as EDEM as a particle template, and then fill the particles to form the required model [33,34]. The particle size of the particles has a certain influence on the simulation accuracy and simulation calculation time. During simulation, particles are usually magnified by a certain multiple, but the magnification ratio should be selected by trial [35]. The contact can be improved by adjusting the contact parameters to adapt to the situation of particle enlargement during simulation [36]. Therefore, the influence of the particle size on the simulation accuracy and simulation time should be obtained through simulation analysis. Particle size and shape should be determined by balancing simulation efficiency and accuracy [37]. Due to limited computing power, the particle size is often enlarged by a certain factor during simulation, and the reliability of the enlarged particle simulation is verified. Wang, X. measured the soil disturbance characteristics and the test process showed that the soil particles can obtain relatively accurate prediction results at a time of 3–8 mm. They concluded that decreasing the particle radius in the simulation from 5 mm to 3 mm can increase the dissolution time by about 7 times (about 500 h), so the particle size should be fully considered during parameter calibration [38,39].

### 3.2. Particle Density

Particle density can be measured according to the density calculation formula, that is, the mass divided by the volume. For example, the soil can be filled with particles in a container of a certain volume, and the density can be calculated according to the density calculation formula. The water-insoluble material can be used to measure the particle density using the pycnometer method, by immersing the particles in water to obtain their volume, or by consulting the literature [40].

### 3.3. Mechanical Properties of Particles

The shear modulus, Young's modulus, and Poisson's ratio can be determined by a uniaxial compression test or tensile test; the Young's modulus and Poisson's ratio can be determined by calculation; and the shear modulus can be determined by calculation [41–44]. Some materials that are difficult to measure, such as dispersed particles, can be obtained through literature review or through parameter calibration, and the reliability of the parameters can be verified by experiments. The shear modulus of the material was determined by

a fracture test using an impact load cell [45]. When measuring the mechanical properties of particles, it is also expressed as normal stress, shear stress, etc. The bonding bond parameters between particles also have a certain influence on the mechanical properties of macroscopic objects. The parameters of bonding bonds between particles can also be calibrated during compression experiments and cutting experiments.

The Young's modulus and shear modulus, as important mechanical parameters of particles, will affect the stability of the computing timestep and thereby influences the calculation time. It is very important to measure Young's modulus, shear modulus and Poisson's ratio before parameter calibration [46]. Zhou, L. determined the particle size distribution of sand particles by sieving method; measured the mechanical parameters of sand by triaxial compression test; and analyzed the force and particle velocity field of the crawler on a sand road [47,48]. Mousaviraad, M. studied the effects of normal stiffness, shear stiffness, critical normal stress, critical shear stress, and filling sphere radius on the performance of the bonded particle model through uniaxial compression tests by EDEM, including resistance to compressive strength and average stress–strain gradient, by using the triaxial compression test to verify the accuracy of the calibration results. In addition to calibrating the parameters of the bond, the influence of different filler particle radii on the mechanical properties was also analyzed [49]. The parameters of the bond can be obtained by a uniaxial compression test. The parameters include normal stress, shear stress, filling ball radius, contact radius, etc. The reliability of the calibration parameters can be verified by triaxial compression test, compression bending test, and fracture experiments [50–52]. The normal and tangential critical stresses of the HMB model can be calibrated on the basis of uniaxial compression tests [53]. In order to obtain more accurate test data, Kim, Y.S. made a comprehensive testing machine for soil mechanical properties in the field. The direct shear test was used to test the shear stiffness of the soil. The normal stiffness of the soil was tested by the compression test. They pointed out that some cohesive soils showed non-flow properties. It is more appropriate to use a hand-held soil resistance meter for calibration than to use the angle of repose [54].

### 3.4. Measurement of Angle of Repose

The static accumulation angle is often used as the target parameter for material parameter calibration [54], and the measurement methods mainly include the cylinder ascending method and the sidewall collapse method. The dynamic stacking angle can make the particles roll in the drum at a constant speed until it is stable. At this time, there is a certain angle between the particle stack and the horizontal plane, which is called the drum method [55–58] (see Figure 1). The particle piles obtained through the method above all need to measure the angle between boundary and horizontal plane. It is convenient to measure directly with tools, but the accuracy cannot be guaranteed. It is also possible to take pictures and perform image preprocessing and algorithms to detect the angle between the edge line and the horizontal plane to obtain the angle of repose. Roessler T. used the lift method to measure the angle of stacking of stones [59]. The angle of repose is used as the test index by Geng, L., with the friction coefficient as a factor. The sidewall collapse test was carried out to obtain the angle of repose (Figure 2). The steepest climbing test was performed, and the least square method was used to fit the regression equation between the friction coefficient and the angle of repose [60].

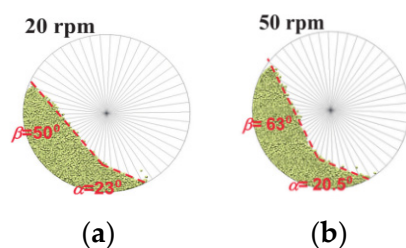
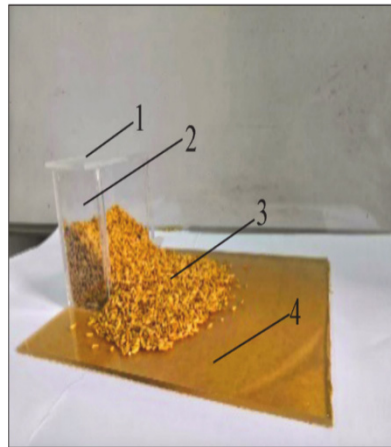
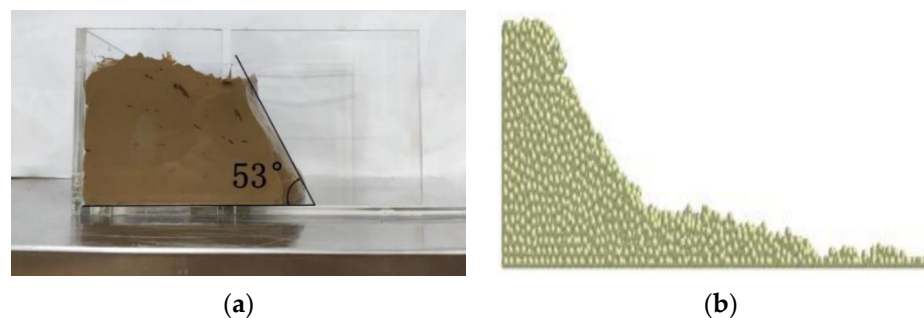


Figure 1. Simulation of dynamic stacking angle (a) 20 rpm; (b) 50 rpm [57].



**Figure 2.** Experimental method of angle of repose formation for baffle lift/collapse method [60]. 1. Side wall; 2. Shell; 3. Oat seeds; 4 Plexiglass plate.

Petingco, M.C. determined the effect of grain shape and contact parameters on the test weight of simulated wheat and developed an efficient wheat grain model for container filling using EDEM, using three different grain models to model wheat grains to determine how grain shape affects bulk density and evaluating six exposure parameters to determine which parameters significantly affect wheat bulk density [61]. Baoyu, Z. used the sidewall collapse method to test the angle of repose of paddy soils and established an EDEM simulation model with Hertz–Mindlin and Johnson–Kendall–Roberts contact models using 11 parameters. On the basis of the Plackett–Burman experiment, it takes the angle of repose as the target parameter to conduct the steepest ascent test and the Box–Behnken test, and it uses the sidewall collapse method to determine the soil angle of repose in the sown field (Figure 3). The reliability of the calibrated parameters was compared and analyzed with the experimental and simulated trench shapes [62].



**Figure 3.** Experiment and simulation of measuring accumulation angle by sidewall collapse method. (a) Experiment; (b) Simulation [62].

The parameter calibration also involves some large particles with irregular shapes. The angle of repose, which is measured by the cylinder lifting method, can also be used as the target parameter for parameter calibration. The angle of repose of the plant stem is measured as shown in Figure 4. A regression model of the angle of repose and the significant parameters was established by using the response surface method [63]. Liang, R. measured the angle of repose of the residual film mixtures with two water content and the static sliding friction angle between the particulate material and the residual film, and carried out the angle of repose test and the inclined plane test to obtain the contact parameters of the residual film mixture particles. The stacking angle of the film mixture was measured by taking pictures and performing edge extraction. The response surface analysis was carried out with the collision restitution coefficient, static friction coefficient,

dynamic friction coefficient, and damping coefficient as the factors and the angle of repose as response (Figure 5) [64].

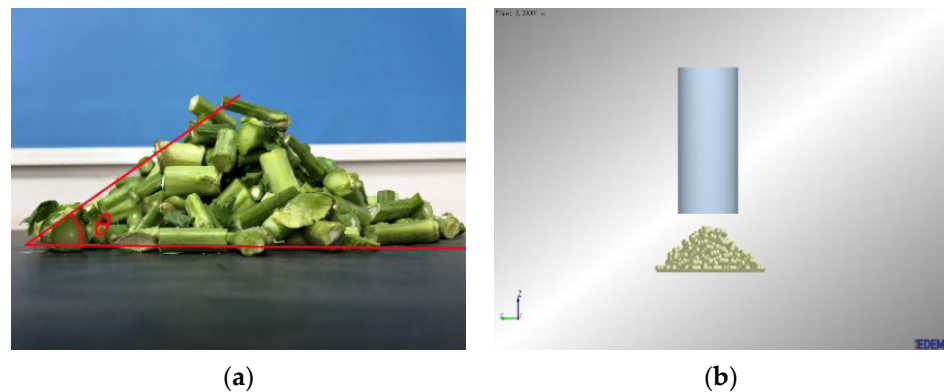


**Figure 4.** Experimental and simulation plots of the stacking angle. (a) Experiment; (b) Simulation [63].

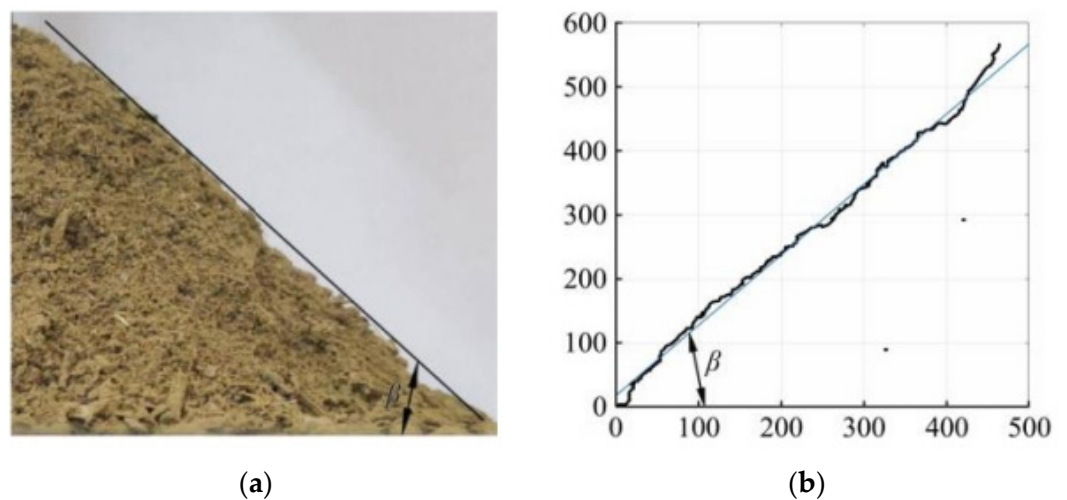


**Figure 5.** Image information of angle of repose edge and extraction and fitting results. (a) Residual film mixture; (b) Edge fitting results [64].

#### 4. Measurement Method of Material Contact Parameters

##### 4.1. Contact Model

##### 4.1.1. Particle–Particle

For DEM simulations of dry soil, the linear spring contact law and the Hertz–Mindlin contact law are mainly used. The Hertz–Mindlin contact law is accurate for contact between spheres, but it has higher computational requirements than the linear model. There are also some specific contact models that can be used for soil simulation, such as hysteretic spring contact law and the Luding contact law. Although, these complex contact laws can be more suitable for complex contact situations, complicating the parameter calibration in the process [65]. The linear spring contact law decomposes the force into a linear component and a damping component, which can further be divided into tangential and normal components; the Hertz–Mindlin contact law divides the force into a nonlinear component and a damping component and the nonlinear components and damping components can be further divided into tangential and normal components. Du, Y. used the method of combining simulation and real experiment to establish accurate faba bean simulated particles and calibrate the parameters. By measuring the 100-grain weight, three-dimensional size, density, and static friction coefficient of Chenghu No. 14 and other parameters, the simulated particles of Chenghu No. 14 broad bean seeds were initially established, and the influence of the static friction coefficient on its accumulation angle was determined during the simulation process [66]. For spherical particles, the Hertz–Mindlin non-slip contact

model is mostly used for non-sticky particles, and the Hertz–Mindlin with bonding, or JKR bonding model, is used for sticky particles as the contact model [67,68]. For complex contacts or more precise requirements for contact parameters, the original contact model can be optimized or the contact model can be customized through an API, for example, Giannis, K. established an “invoking neighboring contact interaction” contact model [69,70].

Due to the certain viscosity between corn and soil particles, Tian, X. used the Hertz–Mindlin with JKR contact model to construct a discrete element simulation model of corn stalk–soil mixture and calibrated the contact parameters of the discrete element simulation [71]. Based on the intrinsic parameters of mung bean seeds, the Hertz–Mindlin with bonding model was used to establish a seed simulation model, and the free fall collision method, the inclined plane sliding method, and the inclined plane rolling method were used to obtain the parameters between the mung bean seed and the contact material [72]. Yuan, Q. conducted simulation analysis and optimization on the sawtooth-shaped fertilizer blade of the organic fertilizer deep applicator and selected the Hertz–Mindlin with bonding model in EDEM to establish the fertilizer block model. And the bonding parameters of the fertilizer block were calibrated by the uniaxial compression test and established a simulation model of single-blade single composting [73]. Chen, G. selected the Hertz–Mindlin non-slip contact model to conduct the sensitivity analysis between single particles and the surface of the machine tool to ensure the accuracy of the wear analysis [74]. Liao, Y. took the stalk of forage rape as the research object, adopted the Hertz–Mindlin with bonding contact model, combined with the bending failure test of forage rape stem, the two-level factor test (screening of significant factors), the steepest slope test, and the response surface test to obtain the bonding parameters such as normal and tangential contact stiffness, and normal and tangential stress. After the parameters are determined, virtual simulation and physical cut-off tests are performed to make sure the reliability of the determined bonding parameters is maintained [75].

#### 4.1.2. Particle–Rigid Body

The particle–rigid body contact model usually adopts the Hertz–Mindlin model. The contact bond adopts the linear elastic contact mode. When the particle is not sticky, the particle–rigid body adopts the non-slip contact form. When the particle itself is sticky, a contact model with certain viscous effects, such as Hertz–Mindlin with bonding, will be used. Verifying the reliability of the contact model and parameters after all parameters are determined is necessary.

Saunders performed DEM simulations to analyze the performance of moldboard skimmers in a cohesive soil bin environment, and a hysteresis spring contact model was used for soil–tool interaction modeling [76]. HMCM (Hertz–Medlin model) and PBCM (parallel build) can be used as cohesive particle–particle contact models and can also be used to simulate soil–tool interactions. Compressible materials such as soil can use HSCM (Hysteresis Spring Contact Model) modeling, which is less used for particle–rigid body modeling, and HSCM is more suitable as a soil–tillage tool contact model [77]. Hertz–Mindlin (HM) contact physics laws with parallel bonds can be used for DEM calculations of forces and displacements of interacting soil and soil tool (steel) elements [78]. In analyzing soil–straw–tool interactions, soil–soil interactions were designated as parallel bond contacts to account for the stickiness of agricultural soils. All other interactions, including straw–straw, soil–straw, soil–tool and straw–tool interactions, are specified as linear contact models [79]. The viscous particle–particle usually adopts the parallel bond contact form, and the particle–tool adopts the linear elastic contact form, and the contact bond only works when the contact distance is less than zero [80].

### 4.2. Friction Coefficient

#### 4.2.1. Static Friction Coefficient

##### (1) Particle–Particle Static Friction Coefficient

The static friction coefficient is often measured by the slope method, and the rolling friction coefficient is measured by the slip test method. Within a certain range, the accumulation angle will increase with the increase in rolling friction coefficient [81]. The coefficient of static friction between particles can be measured through experiments using an instrument, and the angle of repose can also be used as a target parameter for parameter calibration. When the particle–particle static friction coefficient is directly measured by the test method, the particles are pasted on the surface of the flat plate and the particle–rigid static friction coefficient test method is used to obtain the static friction coefficient between particles; when using an instrument to obtain the static friction coefficient between particles, e.g., instruments such as reciprocating pin-type tribometers, two particles are in face-to-face contact during testing [82]. When performing parameter calibration, measuring the intrinsic parameters of the particles in advance is necessary, and using the angle of repose as the target parameter to simulate is the best way to find the best parameters, and ensure the reliability of the parameters combined with the experiment after the parameters are obtained.

## (2) Particle–Rigid Body Static Friction Coefficient

When measuring the particle–rigid body static friction coefficient, the particles are placed on the surface of the rigid body, and the initial position of the rigid body plate is horizontal, so that it rotates around one side of the plate until the particles placed on the plate begin to slide, and the angle between the plate and the horizontal plane is measured. The angle at this time is the particle–rigid body static friction coefficient, which is called the sliding method. The sliding method is the most commonly used method to obtain the static friction coefficient.

Song, S. chose the Hertz–Mindlin non-slip contact model as the soil contact model and used the stacking test and sliding test methods to carry out the restitution coefficient, rolling friction coefficient, and static friction coefficient between the soil and the layered fertilization device. For calibration, a simulation model of soil and a stratified fertilization device is established under the calibrated parameters and verified by actual accumulation tests and sliding tests (Figure 6); the soil sample sampling method adopted is the five-point sampling method, and the soil particle size measurement method is the soil sieve. The density is measured by a volumetric method using a ring knife and balance tool [83]. Liu, W. used the Hertz–Mindlin non-sliding contact mechanical model to calibrate the parameters of micro-potatoes. They used the drop method to measure the collision restitution coefficient of potatoes and steel plates; the suspension collision method to confirm the particle–particle collision restitution coefficient; and the static friction by the sliding method. The coefficient of rolling friction was measured by the slope method, and the angle of repose of the particles was measured by the sidewall collapse method [84]. Yu, Q. used a 3D scanner to scan *Panax notoginseng* seeds to obtain point cloud data and establish a 3D model of the seeds, and used a collision bounce test (free fall method) to measure the coefficient of collision recovery. The four seeds were bound into a plane and the sliding-off method was used to confirm the static friction coefficient. The slope test was used to confirm the rolling friction coefficient. The angle of repose and bench test were used to confirm the reliability of the calibration parameters [85].

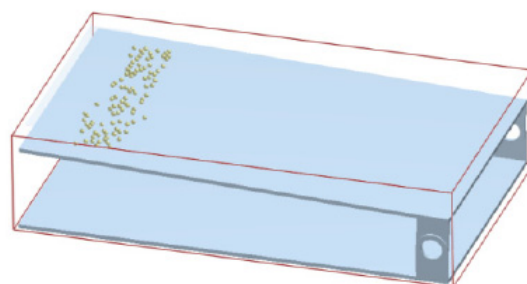


**Figure 6.** Soil slip simulation test [83].

#### 4.2.2. Dynamic Friction Coefficient

##### (1) Particle–Particle Dynamic Friction Coefficient

The static angle of repose is generally used to calibrate the particle–particle rolling friction coefficient, and the funnel method can be used to measure the static angle of repose [86]. For materials that are easier to paste, the materials can be pasted on a flat plate and measured according to the particle–rigid body rolling friction coefficient measurement method. The accumulation angle test can be used to measure the coefficient of rolling friction between soil particles and particles, and the slope test can be used to confirm the coefficient of rolling friction between the soil and the tools. Although the particle–particle rolling friction coefficient can be obtained by the test method, the measurement method is complicated and the results are inaccurate. The method of virtual simulation parameter calibration is often used to confirm the particle–particle rolling friction coefficient, and the parameters are continuously changed until the angles match.

##### (2) Particle–Rigid Body Dynamic Friction Coefficient

The static friction coefficient is obtained by the sliding method, and the rolling friction coefficient (dynamic friction coefficient) is measured by the slope method. The friction coefficient has a great influence on the accumulation angle and is difficult to measure accurately, so they are usually classified as parameters to be calibrated [87,88]. During parameter calibration, the virtual simulation parameters of the parameters are continuously modified until the angle of repose is basically consistent with the test parameters. In addition to the test method for parameter calibration, a machine learning neural network algorithm can also be developed to adapt the parameter calibration process to make the process efficient. Tripathi, A. analyzed the influence of the rolling friction coefficient on the dynamic accumulation angle of different shapes and particles by image analysis and obtained a relatively accurate rolling friction coefficient without parameter calibration [89]. Wang, Y. established a mathematical regression model to actively search for target parameters based on the stacking test method, and calibrated the coefficient of static friction and the coefficient of rolling friction of the corn seed particle model [90]. Ma, S. confirmed the contact parameters between soil particles based on the accumulation angle and used the funnel method to determine the accumulation angle of the tested soil. The soil accumulation angle was used as the test index. A four-factor universal rotation center combined simulation test was carried out; for determination of the coefficient of rolling friction, a slip-down test apparatus was used (see Figure 7) [91].

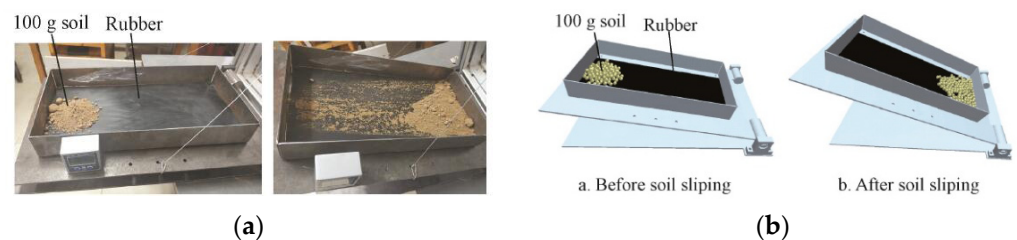


**Figure 7.** Sliding test and simulation test of soil on rubber. (a) Sliding test; (b) Simulation test [91].

In order to measure the contact parameters between clay and soil-contacting parts, Li, J. used the Box–Behnken method in the Design-Expert software to carry out the experimental design of the simulation parameter calibration of the inclined plane test (Figure 8), and used the inclined plane method to obtain the particle–rigid body rolling friction coefficient [92].

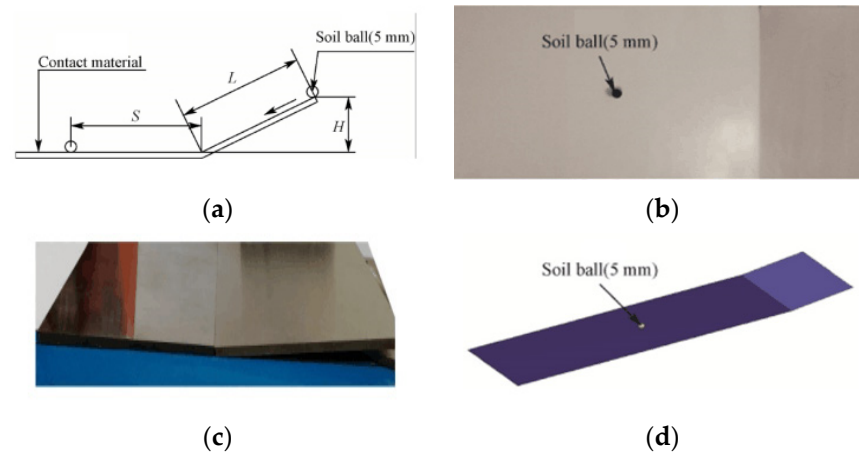


**Figure 8.** Slope test of soil with different contact materials. (a) Principle of slope test; (b) Slope test of 65 MN plate; (c) Slope test of PTFE plate; (d) EDEM simulation slope test [92].

The relationship between the calibration parameters and the response parameters can be established through machine learning methods to determine the mathematical relationship between the two, and machine algorithms can be used to achieve parameter calibration for different materials [93–95]. For example, a BP neural network is used to realize the self-adaptation between particle parameters and particle properties [96]. Zhou, H. used the angle of repose and bulk density of expanded graphite particles as responses, taking particle density, sliding friction, coefficient of restitution, and Poisson's ratio as microscopic variables, and using the self-Adaptive Simulated Annealing optimization algorithm to establish a radial basis function neural network approximation model between microscopic variables and macroscopic responses [97]. Kriztian, K. studied particle velocities, contact forces, and positions of bond breakage during simulation calculations [98].

#### 4.2.3. Collision Restitution Coefficient

##### (1) Restitution Coefficient of Particle–Particle Collision

The particle–particle collision restitution coefficient is usually measured by the suspension collision method. Two particles are suspended in the same vertical plane by a rope, and one of the particles is pulled to a certain height so that it falls toward the other particle, and the collision is recorded by a high-speed camera. The speed or height of the front and rear particles can be calculated to obtain the collision recovery coefficient; in the simulation, a smooth pipe can be used instead of a rope to conduct a collision test, so that the particles with the same shape can collide head-on and calculate the speed ratio [99]. Different test plans can be set based on the collision principle, and the particle–particle collision restitution coefficient is often used as a parameter to be calibrated for parameter calibration experiments.

Qi, J. made walnuts fall from a certain height, measured them with a high-speed camera, and calculated the collision restitution coefficient. Another method of measuring the collision restitution coefficient is as follows (Figure 9): hang two walnuts on a rope and place one of them after raising it to a certain height, put it down, with a ruler next to it, use the height camera to record the height of each stage, and calculate the collision recovery coefficient between the two walnuts [100]. The suspension crash method can be used for crash restitution coefficients of different shapes and sizes [101]. Wang, L. adopted the drop method and the suspension impact method to measure the impact recovery coefficient of hard corn particles (Figure 10) [102,103].

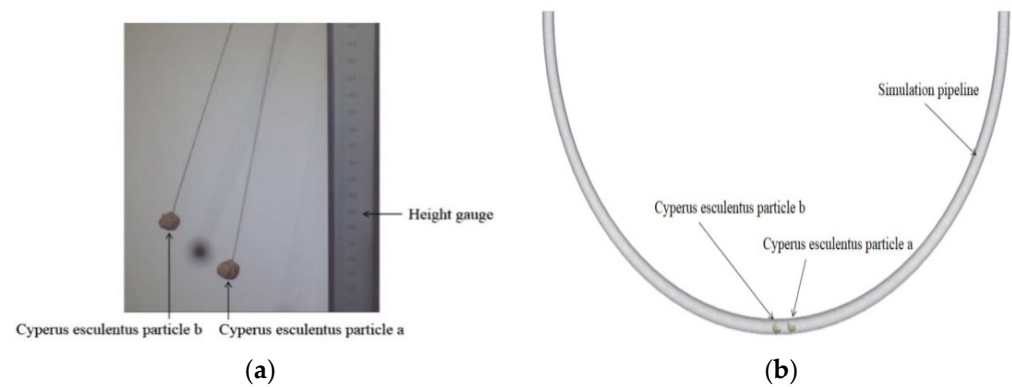


**Figure 9.** Test and simulation test diagram of walnut crash coefficient of recovery. (a) Test; (b) Simulation [100].

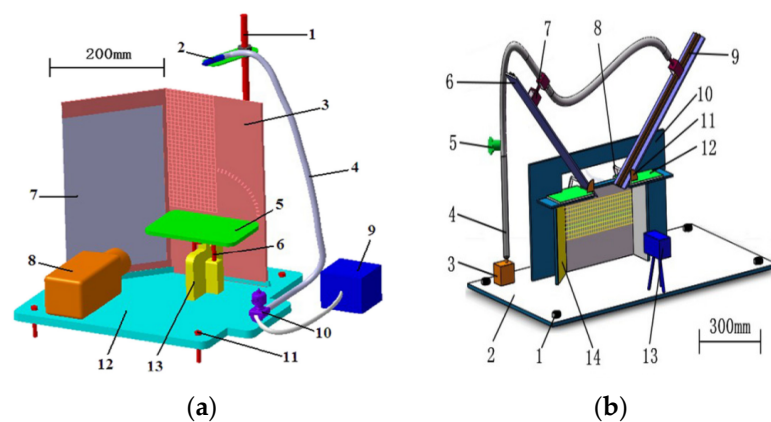


**Figure 10.** The device for measuring the coefficient of restitution by the drop method and the particle collision method. (a) Drop method; (b) Particle collision method [102].

## (2) Restitution Coefficient of Particle–Rigid Body Collision

The particle–rigid body collision restitution coefficient is obtained by the oblique impact method or the drop method. The particle is free to fall at a certain height above the inclined plane; its rebound and velocity direction will change after colliding with the inclined plane. The speed of the particles before and after the collision will be recorded with a high-speed camera. The falling method is performed by placing the particles at a certain height on the horizontal plane to make them fall freely, recording their speed before and after the collision, and calculating the collision recovery coefficient.

Adilet, S. determined the elastic recovery coefficient through a drop test. The calculation method is to divide the drop height by the bounce height to determine the collision recovery coefficient. The particles fall one by one through the turntable (Figure 11a), hit the inclined plate at a certain height, and bounce off after reflection (Figure 11b). After falling to the ground, the collision recovery coefficient can be obtained by calculation [104]. The test method for the elastic recovery coefficient of briquette particles is to make the briquette particles fall freely from the top of an inclined plane. This method is called the oblique impact method (Figure 12). The collision recovery coefficient can be obtained by calculation [105]. Wang, L. proposed a method to confirm the COR value of the collision of irregular particles with a three-dimensional inclined wall, using an oblique impact to make the particles move in both tangential and normal directions to measure the collision restitution coefficient of corn, selecting three corn shapes to study the COR of maize [106].

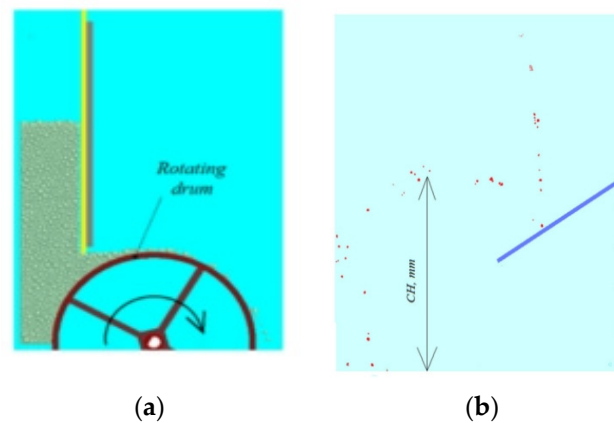


Figure 11. Particle drop test graph. (a) Rotation part; (b) Particle rebound part [105].

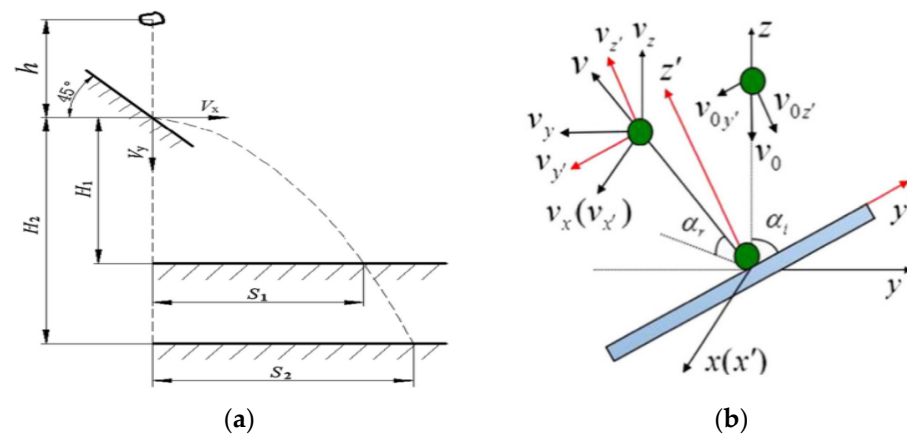


Figure 12. Schematic diagram of the device for testing the coefficient of restitution by the oblique impact method. (a) Two-dimension rebound [105]; (b) Three-dimension rebound [106].

## 5. Summary of Current Research Status and Research Prospects

### 5.1. Summary of the Current Situation

- (1) Parameter calibration has become normative process, including the measurement of intrinsic parameters of materials and the method of parameter calibration through virtual simulation. The intrinsic parameters can often be directly measured by the test method before parameter calibration, and the contact parameters can be obtained by test measurement or parameter calibration through virtual simulation. Usually, the particle–particle static friction coefficient, particle–particle dynamic friction coefficient, and restitution coefficient of particle–particle collision can be obtained by virtual parameter calibration. The particle–rigid body static friction coefficient, particle–rigid body dynamic friction coefficient, restitution coefficient of particle–rigid body collision is usually measured experimentally. When the intrinsic properties of materials are difficult to obtain by direct measurement, they can also be obtained through parameter calibration. The particle–rigid body static friction coefficient is mainly measured by the sliding test method, and the particle–rigid body rolling friction coefficient is measured by the slope method.
- (2) Parameter calibration generally takes the angle of repose as the target parameter. The static angle of repose generally adopts the cylinder lifting method or the side wall lifting method, and the dynamic angle of repose is often measured by the drum method. Due to limitations in terms of computing power, the particle size is often enlarged by a certain number during simulation. Since the particle shape, size and other factors during simulation are slightly different from the actual factor values, and taking into account of the complexity of the actual application environment,

the parameters obtained by calibration have some errors when compared with the actual parameters.

- (3) The Plackett–Burman test method or the rotating center combination test method are the commonly used measures to screen significant factors, and the steepest climbing test and the Box–Behnken test are usually used to calibrate the parameters.
- (4) By simulating the stacking angle test, slope test, sliding test, crash test, etc., and comparing the error with the test results, the purpose of parameter calibration and reliability verification is achieved. The software used for parameter calibration are EDEM, ROCKY DEM, etc. Function expansion of the software is usually carried out by means of the API program.

### 5.2. Prospects

- (1) When the parameters are calibrated, the tools used to measure the particle parameters are not uniform enough, and the differences in the tools easily cause errors in the parameter calibration. If the tools for material parameter measurement can be gradually formed into standards, the accuracy and efficiency of parameter calibration will be improved. If the common calculation theories of parameter calibration are summarized and shared in papers, the efficiency and convenience of parameter calibration will be improved.
- (2) The particle size has a greater impact on the simulation calculation time and simulation accuracy. Due to the computational limitations, the particle size is often enlarged by a certain multiple, but the simulation accuracy and the time saved after amplification need to be further compared to improve the simulation efficiency and simulation accuracy in order to quantify the impact of particle size on the time and simulation efficiency for easy analysis. With the improvement of computing performance, the shape and particle size of simulated particles will be more similar to the actual particles, and the contact situation will be closer to the real situation; then, the simulation's accuracy will be further improved.
- (3) The functions of discrete element simulation software need improvement; many parameter calibration tools need to write an API to operate and the post-processing tools need to be further improved. With the continuous improvement of element simulation software functions, the convenience of discrete element simulation will be improved.

**Author Contributions:** Conceptualization: W.F., X.W. and D.H. reviewed the literature and wrote the initial draft of the paper with assistance from D.H. with X.W.; X.W. and X.C. contributed to revising the manuscript. All authors have read and agreed to the published version of the manuscript.

**Funding:** This work was supported by the National Natural Science Foundation of China (No. 52105304), project of the Agricultural Equipment Department of Jiangsu University (No. NZXB20200104), the Priority Academic Program Development of Jiangsu Higher Education Institutions (No. PAPD-2018-87).

**Institutional Review Board Statement:** Not applicable.

**Data Availability Statement:** Not applicable.

**Conflicts of Interest:** The authors declare no conflict of interest.

## References

1. Li, C.; Yin, H.; Wu, C. Calibration of the Discrete Element Method and Modeling of Shortening Experiments. *Front. Earth Sci.* **2021**, *9*, 636512. [[CrossRef](#)]
2. Syed, Z.; Tekeste, M.; White, D. A coupled sliding and rolling friction model for DEM calibration. *J. Terramech.* **2017**, *72*, 9–20. [[CrossRef](#)]
3. Qu, T.; Feng, Y.; Zhao, T.; Wang, M. A hybrid calibration approach to Hertz-type contact parameters for discrete element models. *Int. J. Numer. Anal. Methods Geomech.* **2020**, *44*, 1281–1300. [[CrossRef](#)]
4. Keppler, I.; Bablena, A.; Salman, N.D.; Kiss, P. Discrete element model calibration based on in situ measurements. *Eng. Comput.* **2021**, *39*, 1947–1961. [[CrossRef](#)]

5. Wang, X.; Li, J. Simulation of triaxial response of granular materials by modified DEM. *Sci. China-Phys. Mech. Astron.* **2014**, *57*, 2297–2308. [[CrossRef](#)]
6. Schramm, M.W.; Tekeste, M.Z.; Steward, B.L. Simulation of uniaxial compression for flexible fibers of wheat straw using the discrete element method. *Trans. Asabe* **2021**, *64*, 2025–2034. [[CrossRef](#)]
7. Chen, Z.; Wang, G.; Xue, D. An approach to calibration of BPM bonding parameters for iron ore. *Powder Technol.* **2021**, *381*, 245–254. [[CrossRef](#)]
8. Mak, J.; Chen, Y.; Sadek, M.A. Determining parameters of a discrete element model for soil-tool interaction. *Soil Tillage Res.* **2012**, *118*, 117–122. [[CrossRef](#)]
9. Wang, X.; Gao, P.; Yue, B.; Shen, H.; Fu, Z.; Zheng, Z.; Zhu, R.; Huang, Y. Optimization of installation parameters of subsoiler' wing using the discrete element method. *Comput. Electron. Agric.* **2019**, *162*, 523–530. [[CrossRef](#)]
10. Zhao, L.; Zhou, H.; Xu, L.; Song, S.; Zhang, C.; Yu, Q. Parameter calibration of coconut bran substrate simulation model based on discrete element and response surface methodology. *Powder Technol.* **2022**, *395*, 183–194. [[CrossRef](#)]
11. Dai, Z.; Wu, M.; Fang, Z.; Qu, Y. Calibration and Verification Test of Lily Bulb Simulation Parameters Based on Discrete Element Method. *Appl. Sci.* **2021**, *11*, 10749. [[CrossRef](#)]
12. Cheng, J.; Zheng, K.; Xia, J.; Liu, G.; Jiang, L.; Li, D. Analysis of adhesion between wet clay soil and rotary tillage part in paddy field based on discrete element method. *Processes* **2021**, *9*, 845. [[CrossRef](#)]
13. Yang, Y.; Wen, B.; Ding, L.; Li, L.; Chen, X.; Li, J. Soil particle modeling and parameter calibration for use with discrete element method. *Trans. Asabe* **2021**, *64*, 2011–2023. [[CrossRef](#)]
14. Refahi, A.; Aghazadeh Mohandesi, J.; Rezai, B. Comparison between bond crushing energy and fracture energy of rocks in a jaw crusher using numerical simulation. *J. S. Afr. Inst. Min. Metall.* **2009**, *109*, 709–717.
15. Xie, C.; Yang, J.; Wang, B.; Zhuo, P.; Li, C.; Wang, L. Parameter calibration for the discrete element simulation model of commercial organic fertilizer. *Int. Agrophys.* **2021**, *35*, 107–117. [[CrossRef](#)]
16. Peng, C.; Xu, D.; He, X.; Tang, Y.; Sun, S. Parameter calibration of discrete element simulation model for pig manure organic fertilizer treated with *Hermetia illucen*. *Trans. Chin. Soc. Agric. Eng.* **2020**, *36*, 212–218.
17. Wang, L.; Fan, S.; Cheng, H. Calibration of contact parameters for pig manure based on EDEM. *Trans. Chin. Soc. Agric. Eng.* **2020**, *36*, 95–102.
18. Shi, L.; Zhao, W.; Sun, W. Parameter calibration of soil particles contact model of farmland soil in northwest arid region based on discrete element method. *Trans. Chin. Soc. Agric. Eng.* **2017**, *33*, 181–187.
19. Zhang, R.; Jiao, W.; Zhou, J.; Qi, B.; Liu, H.; Xia, Q. Parameter Calibration and Experiment of Rice Seeds Discrete Element Model with Different Filling Particle Radius. *Trans. Chin. Soc. Agric. Mach.* **2020**, *51*, 227–235.
20. Shi, G.; Li, J.; Ding, L. Calibration and Tests for the Discrete Element Simulation Parameters of Fallen Jujube Fruit. *Agriculture* **2022**, *12*, 38. [[CrossRef](#)]
21. Xiang, W.; Wu, M.; Lü, J.; Quan, W.; Ma, L.; Liu, J. Calibration of simulation physical parameters of clay loam based on soil accumulation test. *Trans. Chin. Soc. Agric. Eng.* **2019**, *35*, 116–123.
22. Zhang, T.; Zhao, M.; Liu, F. A Discrete Element Method Model of Corn Stalk and Its Mechanical Characteristic Parameters. *Bioresources* **2020**, *15*, 9337–9350. [[CrossRef](#)]
23. Zhang, S.; Tekeste, M.Z.; Li, Y.; Gaul, A.; Zhu, D.; Liao, J. Scaled-up rice grain modelling for DEM calibration and the validation of hopper flow. *Biosyst. Eng.* **2020**, *194*, 196–212. [[CrossRef](#)]
24. Tekeste, M.Z.; Mousaviraad, M.; Rosentrater, K.A. Discrete element model calibration using multi-responses and simulation of corn flow in a commercial grain auger. *Trans. Asabe* **2018**, *61*, 1743–1755. [[CrossRef](#)]
25. Rorato, R.; Arroyo, M.; Gens, A.; Ando, E.; Viggiani, G. Image-based calibration of rolling resistance in discrete element models of sand. *Comput. Geotech.* **2021**, *131*, 103929. [[CrossRef](#)]
26. Binelo, M.O.; Lima, R.F.; Khatchaturian, O.A.; Stransky, J. Modelling of the drag force of agricultural seeds applied to the discrete element method. *Biosyst. Eng.* **2019**, *178*, 168–175. [[CrossRef](#)]
27. Hanley, K.J.; Sullivan, C.; Byrne, E.P.; Cronin, K. Discrete element modelling of the quasi-static uniaxial compression of individual infant formula agglomerates. *Particuology* **2012**, *10*, 523–531. [[CrossRef](#)]
28. Chen, J.; Gao, R.; Liu, Y. Numerical study of particle morphology effect on the angle of repose for coarse assemblies using DEM. *Adv. Mater. Sci. Eng.* **2019**, *2019*, 8095267. [[CrossRef](#)]
29. Shulkin, V.M.; Strukov, A.Y. Particle-Size Analysis of Modern Bottom Sediments by the Laser Diffraction and Sieve Methods. *Russ. J. Pac. Geol.* **2020**, *14*, 378–386. [[CrossRef](#)]
30. Qiu, W.; Hu, W.; Curtin, D.; Motoi, L. Soil particle size range correction for improved calibration relationship between the laser-diffraction method and sieve-pipette method. *Pedosphere* **2021**, *31*, 134–144. [[CrossRef](#)]
31. Kursun, I. Particle size and shape characteristics of kemerburgaz quartz sands obtained by sieving, laser diffraction, and digital image processing method. *Miner. Process. Extr. Metall. Rev.* **2009**, *30*, 346–360. [[CrossRef](#)]
32. Wang, W.P.; Liu, J.L.; Zhang, J.B. Evaluation of Laser Diffraction Analysis of Particle Size Distribution of Typical Soils in China and Comparison with the Sieve-Pipette Method. *Soil Sci.* **2013**, *178*, 194–204. [[CrossRef](#)]
33. Boikov, A.; Savelev, R.; Payor, V.; Potapov, A. Universal approach for DEM parameters calibration of bulk materials. *Symmetry* **2021**, *13*, 1088. [[CrossRef](#)]

34. Cabisco, R.; Finke, J.H.; Kwade, A. Calibration and interpretation of DEM parameters for simulations of cylindrical tablets with multi-sphere approach. *Powder Technol.* **2018**, *327*, 232–245. [[CrossRef](#)]
35. Coetzee, C.J. Particle upscaling: Calibration and validation of the discrete element method. *Powder Technol.* **2019**, *344*, 487–503. [[CrossRef](#)]
36. Roessler, T.; Katterfeld, A. Scaling of the angle of repose test and its influence on the calibration of DEM parameters using upscaled particles. *Powder Technol.* **2018**, *330*, 58–66. [[CrossRef](#)]
37. Rozbroj, J.; Zegzulka, J.; Necas, J.; Jezerska, L. Discrete element method model optimization of cylindrical pellet size. *Processes* **2019**, *7*, 101. [[CrossRef](#)]
38. Wang, X.; Zhang, S.; Pan, H.; Zheng, Z.; Huang, Y.; Zhu, R. Effect of soil particle size on soil-subsoiler interactions using the discrete element method simulations. *Biosyst. Eng.* **2019**, *182*, 138–150. [[CrossRef](#)]
39. Combarros, M.; Feise, H.J.; Zetzener, H.; Kwade, A. Segregation of particulate solids: Experiments and DEM simulations. *Particuology* **2014**, *12*, 25–32. [[CrossRef](#)]
40. Höhner, D.; Wirtz, S.; Scherer, V. Experimental and numerical investigation on the influence of particle shape and shape approximation on hopper discharge using the discrete element method. *Powder Technol.* **2013**, *235*, 614–627. [[CrossRef](#)]
41. Just, S.; Toschkoff, G.; Funke, A.; Djuric, D.; Scharer, G.; Khinast, J.; Knop, K.; Kleinebudde, P. Experimental analysis of tablet properties for discrete element modeling of an active coating process. *AAPS PharmSciTech* **2013**, *14*, 402–411. [[CrossRef](#)] [[PubMed](#)]
42. Ji, S.; Karlovsek, J. Calibration and uniqueness analysis of microparameters for DEM cohesive granular material. *Int. J. Min. Sci. Technol.* **2022**, *32*, 121–136. [[CrossRef](#)]
43. Guo, W.; Hu, C.; He, X.; Wang, L.; Hou, S.; Wang, X. Construction of virtual mulch film model based on discrete element method and simulation of its physical mechanical properties. *Int. J. Agric. Biol. Eng.* **2020**, *13*, 211–218. [[CrossRef](#)]
44. Liu, G.; Xia, J.; Zheng, K.; Cheng, J.; Du, J.; Li, D. Effects of moisture content and tillage methods on creep properties of paddy soil. *PLoS ONE* **2021**, *16*, e0253623. [[CrossRef](#)] [[PubMed](#)]
45. Barrios, G.K.P.; Mde Carvalho, R.; Kwade, A.; Tavares, L.M. Contact parameter estimation for DEM simulation of iron ore pellet handling. *Powder Technol.* **2013**, *248*, 84–93. [[CrossRef](#)]
46. Paulick, M.; Morgeneyer, M.; Kwade, A. Review on the influence of elastic particle properties on DEM simulation results. *Powder Technol.* **2015**, *283*, 66–76. [[CrossRef](#)]
47. Zhou, L.; Gao, J.; Li, Q.; Hu, C.; Wang, R. Numerical simulation analysis of interaction model between track and sandy road based on discrete element method. In Proceedings of the International Conference on Automation and Computing (ICAC), Lancaster University, Lancaster, UK, 7 May 2019.
48. Zeng, H.; Xu, W.; Zang, M.; Yang, P.; Guo, X. Calibration and validation of DEM-FEM model parameters using upscaled particles based on physical experiments and simulations. *Adv. Powder Technol.* **2020**, *31*, 3947–3959. [[CrossRef](#)]
49. Mousaviraad, M.; Tekeste, M.; Rosentrater, K.A. calibration and validation of a discrete element model of corn using grain flow simulation in a commercial screw grain auger. *Trans. Asabe* **2017**, *60*, 1403–1416. [[CrossRef](#)]
50. Liu, F.; Zhang, J.; Chen, J. Modeling of flexible wheat straw by discrete element method and its parameters calibration. *Int. J. Agric. Biol. Eng.* **2018**, *11*, 42–46. [[CrossRef](#)]
51. Ghodki, B.M.; Kumar, K.C.; Goswami, T.K. Modeling breakage and motion of black pepper seeds in cryogenic mill. *Adv. Powder Technol.* **2018**, *29*, 1055–1071. [[CrossRef](#)]
52. Wang, Y.; Zhang, Y.; Yang, Y. Discrete element modelling of citrus fruit stalks and its verification. *Biosyst. Eng.* **2020**, *200*, 400–414. [[CrossRef](#)]
53. Ding, Q.; Ren, J.; Adam, B.E.; Zhao, J.; Ge, S.; Li, Y. DEM analysis of subsoiling process in wet clayey paddy soil. *Trans. Chin. Soc. Agric.* **2017**, *48*, 38–48. (In Chinese with English abstract)
54. Kim, Y.S.; Siddique, M.A.A.; Kim, W.S. DEM simulation for draft force prediction of moldboard plow according to the tillage depth in cohesive soil. *Comput. Electron. Agric.* **2021**, *189*, 106368. [[CrossRef](#)]
55. Hoshishima, C.; Ohsaki, S.; Nakamura, H.; Watano, S. Parameter calibration of discrete element method modelling for cohesive and non-spherical particles of powder. *Powder Technol.* **2021**, *386*, 199–208. [[CrossRef](#)]
56. Coetzee, C. Calibration of the discrete element method: Strategies for spherical and non-spherical particles. *Powder Technol.* **2020**, *364*, 851–878. [[CrossRef](#)]
57. Marigo, M.; Stitt, E.H. Discrete Element Method (DEM) for Industrial Applications: Comments on Calibration and Validation for the Modelling of Cylindrical Pellets. *Kona Powder Part. J.* **2015**, *32*, 236–252. [[CrossRef](#)]
58. Kanakabandi, C.K.; Goswami, T.K. Determination of properties of black pepper to use in discrete element modeling. *J. Food Eng.* **2019**, *246*, 111–118. [[CrossRef](#)]
59. Roessler, T.; Richter, C.; Katterfeld, A.; Will, F. Development of a standard calibration procedure for the DEM parameters of cohesionless bulk materials—Part I: Solving the problem of ambiguous parameter combinations. *Powder Technol.* **2019**, *343*, 803–812. [[CrossRef](#)]
60. Geng, L.; Zuo, J.; Lu, F.; Jin, X.; Sun, C.; Ji, J. Calibration and experiment validation of contact parameters for oat seeds for discrete element method simulation. *Appl. Eng. Agric.* **2021**, *37*, 605–614. [[CrossRef](#)]
61. Petingco, M.C.; Casada, M.E.; Maghirang, R.G.; Fasina, O.O.; Chen, Z.; Ambrose, R.P.K. Influence of Particle Shape and Contact Parameters on DEM-Simulated Bulk Density of Wheat. *Trans. Asabe* **2020**, *63*, 1657–1672. [[CrossRef](#)]

62. Zhu, B.; Liu, J.A.; Chen, X.; Yu, J.; Liu, M.; Zhang, Q. Parameter calibration of soil in the poyang lake region based on discrete element method. *Am. J. Biochem. Biotechnol.* **2020**, *16*, 538–548. [[CrossRef](#)]
63. Liao, Y.; Wang, Z.; Liao, Q.; Liang, F.; Liu, J. Calibration of discrete element parameters of fodder rape crop stem at flowering stage. In Proceedings of the 2020 ASABE Annual International Virtual Meeting, St. Joseph, MI, USA, 13–15 July 2020.
64. Liang, R.; Chen, X.; Jiang, P.; Zhang, B.; Meng, H.; Peng, X.; Kan, Z. Calibration of the simulation parameters of the particulate materials in film mixed materials. *Int. J. Agric. Biol. Eng.* **2020**, *13*, 29–36. [[CrossRef](#)]
65. De Pue, J.; Di Emidio, G.; Flores, R.D.V.; Bezuijen, A.; Cornelis, W.M. Calibration of DEM material parameters to simulate stress-strain behaviour of unsaturated soils during uniaxial compression. *Soil Tillage Res.* **2019**, *194*, 104303. [[CrossRef](#)]
66. Du, Y.; Cui, T.; Zhang, D.; Wei, Y.; Yang, R.; Wu, H. Establishment and parameter calibration of broad bean seeds simulation particles in EDEM. In Proceedings of the 2019 ASABE Annual International Meeting, St. Joseph, MI, USA, 7–10 July 2019.
67. Roessler, T.; Katterfeld, A. DEM parameter calibration of cohesive bulk materials using a simple angle of repose test. *Particuology* **2019**, *45*, 105–115. [[CrossRef](#)]
68. Zu, E.; Zhou, P.; Jiang, Z. Discrete element method of coke accumulation: Calibration of the contact Parameter. N. In Proceedings of the 5th IFAC Workshop on Mining, Mineral and Metal Processing (MMM), Shanghai, China, 23–25 August 2018.
69. Giannis, K.; Schilde, C.; Finke, J.H.; Kwade, A. Modeling of high-density compaction of pharmaceutical tablets using multi-contact discrete element method. *Pharmaceutics* **2021**, *13*, 2194. [[CrossRef](#)] [[PubMed](#)]
70. Mudarisov, S.; Farkhutdinov, I.; Khamaletdinov, R.; Khasanov, E.; Mukhametdinov, A. Evaluation of the significance of the contact model particle parameters in the modelling of wet soils by the discrete element method. *Soil Tillage Res.* **2022**, *215*, 105228. [[CrossRef](#)]
71. Tian, X.; Cong, X.; Qi, J.; Guo, H.; Li, M.; Fan, X. Parameter calibration of discrete element model for corn straw-soil mixture in black soil areas. *Trans. Chin. Soc. Agric. Mach.* **2021**, *52*, 100–108+242.
72. Zhang, S.; Zhang, R.; Chen, T.; Fu, J.; Yuan, H. Parameter calibration of mung bean seeds discrete element simulation and verification test of seeding. *Trans. Chin. Soc. Agric. Eng.* **2022**, *53*, 71–79.
73. Yuan, Q.; Xu, L.; Ma, S.; Niu, C.; Wang, S.; Yuan, X. Design and test of sawtooth fertilizer block crushing blade of organic fertilizer deep applicator. *Trans. Chin. Soc. Agric. Eng.* **2020**, *36*, 44–51.
74. Chen, G.; Schott, D.L.; Lodewijks, G. Sensitivity analysis of DEM prediction for sliding wear by single iron ore particle. *Eng. Comput.* **2017**, *34*, 2031–2053. [[CrossRef](#)]
75. Liao, Y.; Liao, Q.; Zhou, Y.; Wang, Z.; Jiang, Y.; Liang, F. Parameters calibration of discrete element model of fodder rape crop harvest in bolting stage. *Trans. Chin. Soc. Agric. Mach.* **2020**, *51*, 73–82.
76. Saunders, C.; Ucgul, M.; Godwin, R.J. Discrete element method (DEM) simulation to improve performance of a mouldboard skimmer. *Soil Tillage Res.* **2021**, *205*, 104764. [[CrossRef](#)]
77. Zeng, Z.; Chen, Y.; Qi, L. Simulation of cotyledon-soil dynamics using the discrete element method (DEM). *Comput. Electron. Agric.* **2020**, *174*, 105505. [[CrossRef](#)]
78. Ajmal, M.; Roessler, T.; Richter, C.; Katterfeld, A. Calibration of cohesive DEM parameters under rapid flow conditions and low consolidation stresses. *Powder Technol.* **2020**, *374*, 22–32. [[CrossRef](#)]
79. Zeng, Z.; Ma, X.; Chen, Y.; Qi, L. Modelling residue incorporation of selected chisel ploughing tools using the discrete element method (DEM). *Soil Tillage Res.* **2020**, *197*, 104505. [[CrossRef](#)]
80. Zhao, H.; Li, H.; Ma, S. The effect of various edge-curve types of plain-straight blades for strip tillage seeding on torque and soil disturbance using DEM. *Soil Tillage Res.* **2020**, *202*, 104674. [[CrossRef](#)]
81. Han, Y.L.; Jia, F.G.; Tang, Y.R.; Liu, Y.; Zhang, Q. Influence of granular coefficient of rolling friction on accumulation characteristics. *Acta Phys. Sin.* **2014**, *63*, 173–179.
82. Chen, Z.; Wassgren, C.; Veikle, E.; Ambrose, K. Determination of material and interaction properties of maize and wheat kernels for DEM simulation. *Biosyst. Eng.* **2020**, *195*, 208–226. [[CrossRef](#)]
83. Song, S.; Tang, Z.; Zheng, X.; Liu, J.; Meng, X.; Liang, Y. Calibration of the discrete element parameters for the soil model of cotton field after plowing in Xinjiang of China. *Trans. Chin. Soc. Agric. Eng.* **2021**, *37*, 63–70.
84. Liu, W.; Jin, H.E.; LI, H.; LI, X.; Zheng, K.; Wei, Z. Calibration of Simulation Parameters for Potato Minituber Based on EDEM. *Trans. Chin. Soc. Agric. Mach.* **2018**, *49*, 125–135, 142.
85. Yu, Q.; Liu, Y.; Chen, X.; Sun, K.; Lai, Q. Calibration and experiment of simulation parameters for panax notoginseng seeds based on DEM. *Trans. Chin. Soc. Agric. Mach.* **2020**, *51*, 123–132.
86. Hoseinian, S.H.; Hemmat, A.; Esehaghbeygi, A.; Shahgoli, G.; Baghbanan, A. Development of a dual sideway-share subsurface tillage implement: Part 1. Modeling tool interaction with soil using DEM. *Soil Tillage Res.* **2022**, *215*, 105201. [[CrossRef](#)]
87. Jia, H.; Deng, J.; Deng, Y. Contact parameter analysis and calibration in discrete element simulation of rice straw. *Int. J. Agric. Biol. Eng.* **2021**, *14*, 72–81. [[CrossRef](#)]
88. Coetzee, C.J.; Els, D.N.J. Calibration of discrete element parameters and the modelling of silo discharge and bucket filling. *Comput. Electron. Agric.* **2009**, *65*, 198–212. [[CrossRef](#)]
89. Tripathi, A.; Kumar, V.; Agarwal, A. Quantitative DEM simulation of pellet and sinter particles using rolling friction estimated from image analysis. *Powder Technol.* **2021**, *380*, 288–302. [[CrossRef](#)]
90. Wang, Y.; Liang, Z.; Zhang, D.; Cui, T.; Shi, S.; Li, K.; Yang, L. Calibration method of contact characteristic parameters for corn seeds based on EDEM. *Trans. Chin. Soc. Agric. Eng.* **2016**, *32*, 36–42.

91. Ma, S.; Xu, L.; Yuan, Q.; Niu, C.; Zeng, J.; Chen, C.; Wang, S.; Yuan, X. Calibration of discrete element simulation parameters of grapevine antifreezing soil and its interaction with soil-cleaning components. *Trans. Chin. Soc. Agric. Eng.* **2020**, *36*, 40–49.
92. Li, J.; Tong, J.; Hu, B.; Wang, H.; Mao, C.; Ma, Y. Calibration of parameters of interaction between clayey black soil with different moisture content and soil-engaging component in northeast China. *Trans. Chin. Soc. Agric. Eng.* **2019**, *35*, 130–140.
93. Westbrink, F.; Elbel, A.; Schwung, A.; Ding, S.X. Optimization of DEM parameters using multi-objective reinforcement learning. *Powder Technol.* **2021**, *379*, 602–616. [[CrossRef](#)]
94. Klejment, P. Application of supervised machine learning as a method for identifying DEM contact law parameters. *Math. Biosci. Eng.* **2021**, *18*, 7490–7505. [[CrossRef](#)]
95. Benvenuti, L.; Kloss, C.; Pirker, S. Identification of DEM simulation parameters by Artificial Neural Networks and bulk experiments. *Powder Technol.* **2016**, *291*, 456–465. [[CrossRef](#)]
96. Ye, F.; Wheeler, C.; Chen, B.; Hu, J.; Chen, K.; Chen, W. Calibration and verification of DEM parameters for dynamic particle flow conditions using a backpropagation neural network. *Adv. Powder Technol.* **2019**, *30*, 292–301. [[CrossRef](#)]
97. Zhou, H.; Hu, Z.; Chen, J.; Lv, X.; Xie, N. Calibration of DEM models for irregular particles based on experimental design method and bulk experiments. *Powder Technol.* **2018**, *332*, 210–223. [[CrossRef](#)]
98. Kotrocz, K.; Kerenyi, G. Investigation the effect of the model dimension in soil-cone penetrometer discrete element simulation. In Proceedings of the 32nd European Conference on Modelling and Simulation (ECMS), Wilhelmshaven, Germany, 22–25 May 2018.
99. Garcia, B.; Richefeu, V.; Baroth, J.; Daudon, D.; Villard, P. Collision of shaped boulders with sand substrate investigated by experimental, stochastic, and discrete approaches. *J. Geophys. Res.-Earth Surf.* **2020**, *125*, e2019JF005500. [[CrossRef](#)]
100. Qi, J.; An, S.; Kan, Z.; Meng, H.; Li, Y.; Zhao, X. Discrete element-based calibration of simulation parameters of *Cyperus esculentus* L. (tiger nut) planted in sandy soil. *J. Food Process. Preserv.* **2021**, *45*, e15631. [[CrossRef](#)]
101. Hlosta, J.; Zurovec, D.; Rozbroj, J.; Ramirez-Gomez, A.; Necas, J.; Zegzulka, J. Experimental determination of particle-particle restitution coefficient via double pendulum method. *Chem. Eng. Res. Des.* **2018**, *135*, 222–233. [[CrossRef](#)]
102. Wang, L.; Wu, B.; Wu, Z.; Li, R.; Feng, X. Experimental determination of the coefficient of restitution of particle-particle collision for frozen maize grains. *Powder Technol.* **2018**, *338*, 263–273. [[CrossRef](#)]
103. Wang, L.; Zheng, Z.; Yu, Y.; Liu, T.; Zhang, Z. Determination of the energetic coefficient of restitution of maize grain based on laboratory experiments and DEM simulations. *Powder Technol.* **2020**, *362*, 645–658. [[CrossRef](#)]
104. Adilet, S.; Zhao, J.; Sayakhat, N.; Chen, J.; Nikolay, Z.; Bu, L.; Wang, Z. Calibration strategy to determine the interaction properties of fertilizer particles using two laboratory tests and DEM. *Agriculture* **2021**, *11*, 592. [[CrossRef](#)]
105. Xia, R.; Li, B.; Wang, X.; Li, T.; Yang, Z. Measurement and calibration of the discrete element parameters of wet bulk coal. *Measurement* **2019**, *142*, 84–95. [[CrossRef](#)]
106. Wang, L.; Zhou, W.; Ding, Z.; Li, X.; Zhang, C. Experimental determination of parameter effects on the coefficient of restitution of differently shaped maize in three-dimensions. *Powder Technol.* **2015**, *284*, 187–194. [[CrossRef](#)]